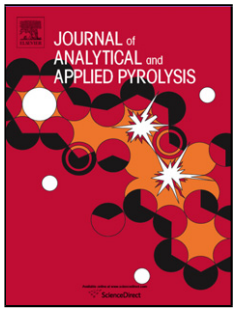

Title: Preparation of activated carbon-metal (hydr)oxide materials by thermal methods. Thermogravimetric-mass spectrometric (TG-MS) analysis

Author: Adrián Barroso-Bogeat María Alexandre-Franco Carmen Fernández-González Vicente Gómez-Serrano

PII: S0165-2370(15)30178-9
DOI: http://dx.doi.org/doi:10.1016/j.jaap.2015.09.004
Reference: JAAP 3566

To appear in: *J. Anal. Appl. Pyrolysis*

Received date: 28-7-2014
Revised date: 4-9-2015
Accepted date: 5-9-2015

Please cite this article as: Adrián Barroso-Bogeat, María Alexandre-Franco, Carmen Fernández-González, Vicente Gómez-Serrano, Preparation of activated carbon-metal (hydr)oxide materials by thermal methods.Thermogravimetric-mass spectrometric (TG-MS) analysis, Journal of Analytical and Applied Pyrolysis http://dx.doi.org/10.1016/j.jaap.2015.09.004

Preparation of activated carbon-metal (hydr)oxide materials by thermal methods. Thermogravimetric-mass spectrometric (TG-MS) analysis

Adrián Barroso-Bogeat, María Alexandre-Franco, Carmen Fernández-González, Vicente Gómez-Serrano* vgomez@unex.es

Departamento de Química Orgánica e Inorgánica, Facultad de Ciencias, Universidad de Extremadura, Avda. de Elvas s/n, 06006 Badajoz, Spain

*Corresponding author. Tel.: +34 924 289421; fax: +34 924 271449.

Highlights

- For the AC-MO materials, the total loss of mass varies between 2.47 and 23.20 wt%.
- Dehydration, dehydroxylation, decarboxylation, carbothermal reduction, etc., occur.
- The number of thermal effects desorbing CO_2 and CO is larger with the metal ions.
- Dehydroxylation is stronger than dehydration only with the Fe^{3+} ion and with TiO_2.
- The masses of evolved gases are much higher for the sample prepared with $SnCl_2$.

Abstract

Activated carbon (AC)-metal (hydr)oxide (MO) materials prepared by wet impregnation of a commercial AC with Al^{3+}, Fe^{3+}, Zn^{2+}, $SnCl_2$, TiO_2 and WO_4^{2-} in water at pH between 1.37 and 9.54 in two successive soaking and oven-drying steps are analysed by thermogravimetry-mass spectrometry (TG-MS) between 25 and 900 ºC. Under identical conditions, a blank sample (ACB) was first prepared using deionized water and then thermally analysed. The mass loss in the TG analysis is 1.35 wt% for AC, 2.12 wt% for ACB, and between 2.47 and 23.20 wt% for the AC-MO materials. For these materials, it depends on the impregnation agent and varies by $SnCl_2 > Fe^{3+} > Al^{3+} > Zn^{2+} > WO_4^{2-} > TiO_2$. The number of thermal effects giving off CO_2 and CO is larger with the Al^{3+}, Fe^{3+} and Zn^{2+} ions than with $SnCl_2$, TiO_2 and WO_4^{2-}. It is so in particular for CO_2 with the Fe^{3+} ion and for CO with the Al^{3+} ion. In general, the release of CO at high temperature has been associated with the carbothermal reduction of metal oxides. As a result of the reaction low-melting point metals such as Al, Zn and Sn, unlike Fe and W, are formed which vaporize and thereby contribute to the mass loss. Only with Fe^{3+} and TiO_2, the amount of desorbed water is larger by dehydroxylation than by dehydration. The masses of evolved H_2O, CO_2 and CO are by far higher with $SnCl_2$, whereas they are lower with TiO_2 and WO_4^{2-}.

Keywords: Activated carbon; Metal ions/metal oxides; Activated carbon-metal (hydr)oxide materials; Thermal behaviour; TG-MS analysis.

1. Introduction

Water treatment is the major liquid-phase application of AC [1]. In the adsorption of solutes from water, an important property of AC is the polarity of its surface because it determines the affinity of the carbon for the adsorptive. For the most part, AC surfaces are nonpolar, making the adsorption of inorganic electrolytes difficult and the adsorption of organics easily effected [2]. In fact, AC has been an effective adsorbent for the removal of many organic substances in water [3]. On the other hand, hydroxo-complexes of multivalent metals are amphoteric in character as they may dissociate protons from coordinatively bound water molecules or they may add protons to hydroxide ions. Thus, the acidity or basicity of the metal hydroxide depends on the polarization of the water molecules or hydroxide ions which depends in turn on the charge and radius of the metal ion [4]. Furthermore, metal oxides have a noticeable degree of ionicity in their metal-oxygen bonding [5]. Therefore, a combination of AC surface and metal (hydr)oxide (MO) properties may give rise to a more versatile adsorbent in adsorption processes and this redounds the number of applications. The surface composition and polarity may be further modified by heat treatment of the resulting samples. Herein, using a series of AC-MO materials prepared by wet impregnation of a commercial AC with Al^{3+}, Fe^{3+}, Zn^{2+}, $SnCl_2$, TiO_2 and WO_4^{2-} in water under mild heating conditions, the present study aims at investigating the thermal behaviour of such materials by thermogravimetric-mass spectrometric (TG-MS) analysis. Thus, valuable information related not only to the preparation of hybrid adsorbents with a tailored composition and presumably associated adsorption properties but also for the purpose of AC and MO regeneration can be obtained.

2. Experimental

2.1. Sample preparation

A granular AC (Merck; Darmstadt, Germany; Cod. 1.02514.1000; 1.5 mm average particle size) and $Al(NO_3)_3 \cdot 9H_2O$, $Fe(NO_3)_3 \cdot 9H_2O$, $Zn(NO_3)_2 \cdot 6H_2O$, $SnCl_2 \cdot 2H_2O$ and $Na_2WO_4 \cdot 2H_2O$ (Panreac; Barcelona, Spain; reagent grade) and anatase powder (Aldrich; Steinheim, Germany; particle size lower than 44 μm) were used. Data obtained in characterization studies of AC are reported elsewhere [6-8]. Deionized water at pH 5.05 was used in the preparation of the impregnation solutions. For these solutions, the pH was measured just after their preparation and obtained values are listed in Table 1.

The preparation of the AC-MO materials was carried as described in detail before [7,8]. With the naked eye no change in the morphology and size of AC particles was observed after the process of preparation of the samples, which proves that under the operating conditions AC is a mechanically resistant material. For comparison purposes, a blank sample (ACB) was also prepared from AC and deionized water by using the same protocol as for the AC-MO materials. The mass change (MC, hereafter) after the preparation of the samples was estimated by the following expression:

$$MC\ (\%) = 100\frac{M_f - M_i}{M_i} \qquad (1)$$

where M_i is the initial mass of AC and M_f is the final mass of impregnated material. The values of MC for the AC-MO materials are set out in Table 1, together with sample codes.

2.2. Sample analysis

The elemental analysis of the samples (C, H, N and S) was performed in an analyser (CHNS-932, LECO), whereas the O content was estimated by difference. The simultaneous thermogravimetric-mass spectrometric (TG-MS) analysis of the samples was performed in a thermobalance (Setsys Evolution-16, Setaram) coupled to a mass spectrometer (Pfeiffer Vacuum, Omnistar), provided with a Faraday type detector. This system operated by evacuating at 2.8 10^{-4} Pa and at a measurable gas pressure of 0.013 Pa. Gases were analysed at time intervals of 0.2 s. Ions of *m/z* 16, 32, 18, 28 and 44 were selected to measure the concentrations of O, O_2, H_2O, CO and CO_2, respectively. Samples of approximately 25 mg were heated from 25 to 900 ºC at 10 ºC·min^{-1} in helium atmosphere (flow rate = 50 mL·min^{-1}). Of the analysed gaseous chemical species, O and O_2 were not detected regardless of the AC-MO material.

3. Results and discussion

3.1. Preparation of the samples

3.1.1. pH of the impregnation solutions

The measured pH for the impregnation solutions (Table 1) varies by $SnCl_2$ < Fe^{3+} < Al^{3+} < water ≈ Zn^{2+} ≈ TiO_2 < WO_4^{2-} and in the wide range from 1.54 for S120 to 9.54 for W120. For the Al^{3+}, Fe^{3+} and Zn^{2+} ions, the pH variation is consistent with the tendency exhibited by these metal ions to hydrolyse [9]. Stannous chloride is readily soluble in water (i.e. 178 g $SnCl_2$/100 g water at 10 ºC [10]), where it may take part in various hydrolysis and oxidation reactions depending on pH [9, 11], concentration [12], presence of aerial oxygen [13], and storage time [14], which provide the aqueous

medium with a high H^+ concentration. Titanium dioxide (anatase) shows a high tendency to hydroxylation [15]. Therefore, after the contact with water already hydroxylated anatase should only undergo a slight hydroxylation, according to the small pH change produced in the TiO_2 suspension with respect to deionized water. The pH of 9.54 measured for the $Na_2WO_4.2H_2O$ solution falls within the range of pH values between 9.15 and 10.5 reported in the literature for molar solutions prepared from $Na_2WO_4.2H_2O$ and purified water [16]. The alkalinity of the WO_4^{2-} solution may be due to the presence of excess alkali (i.e. NaOH) in commercial $Na_2WO_4.\ 2H_2O$ or to Na_2WO_4 hydrolysis and polymerization by the postulated basic mechanism in the formation of iso- and heteropolytungstates from WO_4^{2-} [16].

3.1.2. Mass changes

The MC produced as a result of the process of preparation of ACB was - 4 wt%. Since ACB was prepared using deionized water and the soaking step at 80 ºC was carried out in the absence of air by using a three necked glass flask, the mass decrease must be due to the oxidation of AC by dissolved oxygen. Likely, it affected the organic fraction of AC rather than its inorganic fraction as the determined ash content is 5.14% for AC and 6.64 % for ACB. Furthermore, the FT-IR spectrum for ACB, as prominent differences in respect to the spectrum of AC [6] (i.e. both spectra are plotted in Fig. 1 for comparison purposes), shows the strong bands at 1192 cm^{-1} and 1642 cm^{-1} which are ascribable to the C-O stretching vibration of phenolic hydroxyl groups and to the presence of water in ACB, respectively.

For the AC-MO materials (Table 1), the MC varies widely between + 2 wt% for A120 and + 49 wt% for S120, following the sequence S120 >> F120 > W120 > Z120 =

T120 > A120 and being markedly higher for F120 and very especially for S120 than for the rest of the samples. Probably, the diffusion of the impregnation agent in AC pores during the soaking step at 80 ºC was the most important factor with influence on the MC.

3.2. Chemical analysis of the samples

Data of the elemental analysis (C, H, N, S, O) for AC, ACB, and AC-MO materials are collected in Table 2. They show first that AC, as for typical ACs, is mainly constituted of carbon and also, although much less, of oxygen. However, hydrogen, nitrogen and sulphur are minor heteroatoms in AC. Second, for ACB the H and O contents increase whereas the C and S contents decrease. These results are quite interesting and must be highlighted as they provide further evidence that as a result of the treatment of AC with non-deaerated deionized water oxygen surface groups were formed and also that the process was accompanied with a mass loss that affected the C content. The higher N content for ACB than for AC denotes concentration of this heteroatom in ACB from AC. Third, the variation trends of the C, H, N, S and O contents for the AC-MO materials are generally the same as for ACB. Nevertheless, they are enhanced (C, O) or mitigated (H, N, S) depending on the degree of impregnation of AC. Notice that the H content is much higher for ACB than for the rest of the samples, including AC; whereas the opposite applies to T120. Also it is worth mentioning the markedly higher N content for A120, F120, Z120 and T120 than for AC. For the samples prepared with metal ions, it varies by Z120 > A120 > F120.

3.3. Thermal analysis

3.3.1. AC and ACB

When activated carbon is heat-treated above ambient temperature, particular carbon-oxygen surface functionalities decompose thermally at different characteristic temperatures with gas release [17-19]. For HNO_3-oxidized activated carbon, Szymanski et al. [17] reported that (i.e. the temperature of maximum rate is indicated in parentheses) water gas generates from loosely bound water molecules (up to 127 ºC) and from water H-bonded to oxygen complexes or condensation water from adjacent carboxylic or phenolic groups (above 177 ºC). Carbon dioxide originates from CO_2 chemisorbed in micropores (127 ºC), rearrangements during heating or exposure to the atmosphere (197-237 ºC), single carboxyl groups (277 ºC), single carboxylic structures removed or transformed into anhydrides, lactones or lactols (340 ºC), δ-lactones (517 ºC), and γ-lactones (667 ºC). Carbon monoxide desorbs from carbonyl groups in α-substituted ketones (277 ºC), anhydrides (447 ºC), phenol or hydroquinone groups (567 ºC), and semiquinones or quinones (677 ºC).

From the slope changes in the TG curve for AC in Fig. 2(a) it follows that the heat treatment of AC from room temperature to 900 ºC in helium atmosphere was accompanied with various overlapping effects of weight loss. The mass of sample mainly decreased at 25-275 ºC and 640-900 ºC, whereas the effect of mass reduction was markedly smaller between 350 and 640 ºC. On the other hand, the MS profiles of H_2O, CO and CO_2 are depicted in Fig. 2(b). The broad and strong peak centred at around 225 ºC in the H_2O profile denotes that water desorbed from various water forms and sources, including hydration water, H-bonded water and water generated from oxygen surface groups of AC. Oxygenated groups may contribute as well to the release of CO_2 in accordance with the strong peak exhibited by the CO_2 profile at around 250 ºC. The slope change in the ascending branch of this peak also suggests that CO_2

desorbed from CO_2 chemisorbed in micropores of AC. Although the CO profile displays various sections of increasing slope in the temperature range 445 to 870 ºC, which proves that different CO-desorbing oxygen surface groups decomposed thermally during the heat treatment of AC, the content of such groups was however practically negligible in AC as the mass of evolved CO was as small as 0.010 mg for AC (Table 4).

The TG-DTG curves in Figs. 2(a) and 3(a) show that the maximum of weight loss at 225 ºC for AC splits into two readily visible maxima centred at around 100 and 300 ºC for ACB. In addition, the mass loss above 600 ºC was greater for ACB than for AC. The overall mass loss over the temperature range 25 to 900 ºC was 2.16 wt% for ACB, which is noticeably higher than 1.50 wt% for AC. The MS results for ACB (see Fig. 3(b) and data in Table 4) also show that desorption occurred in the neighbourhood of 125 and 300 ºC for H_2O and almost progressively in the temperature range 200 to 850 ºC for CO. However, the CO_2 profile is very similarly shaped for ACB and AC. The amount of evolved gases is larger by $H_2O > CO_2 > CO$ for AC and by $CO > H_2O > CO_2$ for AC. The total loss of mass was 0.33 mg for AC and 0.60 mg for ACB. In brief, from the MS results obtained for AC and ACB it becomes clear that the oxidation of AC during the preparation of ACB had a beneficial effect on the thermal stability and content of oxygen surface groups desorbing H_2O and CO, respectively.

3.3.2. AC-MO materials

3.3.2.1. Sample A120

The TG curve in Fig. 4(a) shows stronger slope changes in the temperature ranges 80-120 ºC and 200-350 ºC, the maxima of weight decrease being at around 100 and 250 ºC in the DTG curve. At higher temperatures, the mass of sample almost

steadily decreased but the thermal effects were weaker as only two very broad peaks are displayed by the DTG curve in the neighbourhood of 435 and 680 ºC. The mass loss between 25 and 900 ºC was 7.95 wt%, which is markedly higher than 1.35 wt% for AC and 2.16 wt% for ACB (see data in Table 3).

The MS profiles of H_2O, CO_2 and CO are plotted in Fig. 4(b). The H_2O profile displays a very broad peak at 145 ºC that tails up to around 800 ºC. The shape of this peak advocates for water release from various environments. Likely, it was physically adsorbed water and hydroxylation water, involving C-OH groups and Al-OH groups. The C-OH groups may be indigenous groups of AC and groups formed by oxidation of surface structures of AC during the preparation of A120. The Al-OH groups, together with hydration water, should belong to the coordination sphere of the Al^{3+} ion incorporated to AC during the impregnation treatment. With regard to the thermal stability of the Al-OH groups it is relevant to point out here that metastable alumina polymorphs undergo dehydroxylation at low temperatures, i.e. γ-$Al(OH)_3$ (gibbsite), 150-300 ºC; γ-AlOOH (boehmite), 300-500 ºC; α-$Al(OH)_3$ (bayerite), 200-300 ºC [20], which are below approximately 400 ºC (i.e. temperature above which the loss of water greatly decreased in the H_2O profile) and therefore any of the aforesaid polymorphs was susceptible to be formed in the preparation of A120. At higher temperatures, a series of intermediate aluminium oxides are formed before final conversion to corundum, α-Al_2O_3 [21,22].

The MS profile of CO_2 in Fig. 4(b) displays a very broad and strong peak at 270 ºC with two readily visible shoulders at around 400 ºC and 700 ºC. To the evolution of CO_2 in the wide temperature range below 700 ºC likely contributed thermally unstable oxygen surface groups of A120 that desorbed at different temperatures depending on the

group type and its environment [17,19]. The gasification of carbon atoms by oxygen remaining chemisorbed after the oven-drying step in the preparation of A120 may also cause CO_2 release, as for carbonaceous materials the process commences at around 250 ºC and progresses between 250 and 325 ºC [23]. Concerning the oxidation of A120 it should also be borne in mind that the thermolysis of benzene derivatives [24,25] results in radical type intermediates which are very reactive and that may be further degraded with CO_2 release. In connection with the thermal transformation of organic matter it is also pertinent to point out here that an aluminium oxide such as alumina behaves as a catalyst or support in many catalysis processes [26]. Likewise, at high heat treatment temperatures, in accordance with the Ellingham diagram plots CO_2 may be generated by the reaction (2):

$$2CO \rightarrow CO_2 + C \qquad \Delta H = -161 \text{ kJ mol}^{-1} \qquad (2)$$

as suggested by the increased evolution of CO_2 at around 700 ºC while for CO it remained practically constant between 700 and 800 ºC.

As shown in Fig. 4(b) for CO, the evolution of CO started at around 200 ºC, which is worth mentioning as this desorption temperature for CO is far below the previously reported temperature range from *ca.* 500 ºC to *ca.* 1000 ºC [18]. Furthermore, the CO profile exhibits a series of greater slope ascending sections at 150-300, 350-440, 540-700 and 800-850 ºC. Occurrence of various thermal effects in such temperature intervals is indicative of CO desorption from different sources and/or environments. Probably, CO desorbed from phenolic hydroxyl groups of A120 (i.e. indigenous groups of AC and formed by AC oxidation) that underwent thermal decomposition with transformation into cyclohexadienone or phenoxy radical as intermediates and as a last resort with CO ejection [27]. Perhaps, CO was also evolved

by thermal desorption from C-O-Al atomic grouping formed by condensation of different origin –OH groups during the process of preparation of A120. On the other hand, CO may be also originated because of the action of Al_2O_3 on the carbon support at high temperature. Under the conditions of the TG-MS analysis, the heating rate being 10 ºC/min, it is possible that amorphous Al_2O_3, rather than fully crystallized Al_2O_3 phases, was formed transiently and that, because of an enhanced reactivity, it reacted with AC (i.e. the so-called carbothermal reduction of metal oxides) with CO release. This assumption is supported by the fact that the formation of amorphous Al_2O_3 by decomposition of hydrates and nitrates at 400 ºC [28] and by dehydration of gibbsite at 600 ºC was reported elsewhere [29]. From an amorphous precursor, γ-Al_2O_3 was formed and remained present at temperatures as high as 1200 ºC [30,31]. As a result of the carbothermal reduction of Al_2O_3 at high temperature, different carbon-oxygen and aluminium oxygen bonds containing intermediate chemical structures may be formed transiently first and transformed then into CO and Al. Elemental Al should vaporize as this metal melts at 660.32 ºC [10]. In fact, the removal of Al from A120 is corroborated by the determined ash content for A120 and for a sample prepared by heat treatment of A120 at 850 ºC for 2 h, which is equal to 7.11 and 5.68 wt%, respectively. Of course, no thermal effect on the mass of sample is attributable to the carbothermal reduction of α-Al_2O_3 as for this alumina polymorph the process of formation is thermodynamically favourable above 2320 ºC, $\Delta H^0_{298\,k}$ being 1344.1 kJ mol^{-1} [32].

3.3.2.2. Sample F120

As far as the thermal behaviour of F120 is concerned, the TG curve in Fig. 5(a) shows an almost steady mass decrease over the wide temperature interval above

approximately 200 ºC, being extremely greater at around 750 ºC. The DTG curve displays four peaks at 100, 245, 370 and 750 ºC, the last being by far the strongest one. The total loss of mass between 25 and 900 ºC was as high as 12.27 wt%, which is in line with the high MC for this sample (Table 1). In the MS profiles of H_2O, CO_2 and CO in Figs. 5(b) only a very sharp and strong peak centred at around 750 ºC is visible for CO. Therefore, the process of thermal decomposition was very rapid as, despite the dynamic heating in the analysis run, a great mass loss occurred in a narrow temperature range. However, Fig. 5(c) shows various overlapping peaks below 700 ºC, i.e. at 145 and 250 ºC for H_2O, 320, 375 (the strongest one), 465, 540 and 675 ºC for CO_2 and at 350 ºC for CO. At higher temperatures, clearly, the CO profile only exhibits the presence of a shoulder at around 600 ºC.

The effects of water desorption associated with the loss of physically bound water and the release of structurally bound water from F120 take place at somewhat different temperatures from those reported in previous studies for goethite (α-FeOOH) [33] and lepidocrocite (γ-FeOOH) [34], which is attributable to water release by the carbon support. If goethite was found in F120, it may be formed from ferrihydrite [35] that precipitates from Fe^{3+} nitrate solutions. It is a poorly crystalline or amorphous material of ill-defined composition. Perhaps, when heating in the thermal analysis of F120, goethite dehydroxylated according to the reaction (3) [36]:

$$2FeOOH \rightarrow Fe_2O_3 + H_2O \qquad (3)$$

and transformed into hematite (α-Fe_2O_3) or magnetite (Fe_3O_4) at higher temperatures [37]. The reduction of the resulting iron oxide by the carbon support at around 750 ºC may take place by the sequence $Fe_2O_3 \rightarrow Fe_3O_4 \rightarrow FeO \rightarrow Fe$ and with a great CO release. Occurrence of more than a single redox process is proved by the shoulder at

around 600 ºC in the CO profile. However, this lower temperature effect may also be due to the thermal decomposition of C-O-Fe atomic groupings formed by condensation of C-OH groups and Fe-OH groups during the process of preparation of F120. Moreover, the great CO evolution is consistent with the strong CM of + 14 wt% produced in the preparation of F120. For this sample, as for A120, the great desorption of CO_2 below 700 ºC is ascribable to different thermal effects on the mass of sample, as detailed above.

3.3.2.3. Sample Z120

In the TG curve plotted in Fig. 6(a), three greater slope branches are clearly distinguishable with onsets at approximately 40, 160 and 700 ºC. The DTG curve displays four well-defined strong peaks at 90, 210, 270, and 870 ºC. The fact that peculiarly for Z120 three peaks appear at low temperatures is worth mentioning as it may be connected with desorption of water and nitrate anion from zinc hydroxide nitrate, $Zn_5(OH)_8(NO_3)_2.2H_2O$. Perhaps, this hydrate was formed on basic surfaces of AC during the preparation of Z120 and, although transformed into ZnO via $Zn(OH)_2$ [38], to some extent remained in the sample, decomposing when heating in the thermal analysis run. As the temperature increased in this analysis, $Zn_5(OH)_8(NO_3)_2.2H_2O$ should transform first into $Zn_5(OH)_8(NO_3)_2$ and then into ZnO below 300 ºC [39]. For Z120, the mass loss between 25 and 900 ºC was 7.02%. Although to a lesser extent, the presence of metal nitrates in A120 and F120 should not be ruled out as the N content is also high for this couple of samples (Table 2). In fact, it is also suggested by the appearance of the broad maximum at 250 ºC in the DTG curve for A120, which is plotted in Fig. 4(a).

The MS profiles in Fig. 6(b) display maxima or shoulders at 140 ºC for H_2O, 220, 280, 310, 415, 550 and 845 ºC for CO_2, and 220, 315 and 880 ºC for CO. Probably, CO was generated at high temperature because of the reaction (4) [40]:

$$ZnO + C \rightarrow Zn + CO \quad (4)$$

that also gives Zn. In fact, the partial reduction of ZnO in the presence of a dispersive carbon phase at 650 ºC was suggested elsewhere [41]. Furthermore, an additional weight loss above 800 ºC was assigned to a further ZnO reduction. According to the here obtained TG-MS results, the redox process was more favourable above 700 ºC, although it started at lower temperatures. The small amount of CO_2 generated at around 845 ºC may originate by the reaction (2). Since metal zinc melts at 419.53 ºC [9], vaporization should also contribute to the mass decrease produced at high temperatures. Accordingly, the strong effect of mass loss shown by the TG curve in Fig. 6(a) above 750 ºC may be due to the release of CO and also of vaporized Zn.

3.3.2.4. Comparison of A120, F120 and Z120

For the samples prepared with the metal ions, the total loss of mass is higher by F120 > A120 > Z120. The mass of evolved gases varies by F120 > Z120 > A120 > AC for H_2O, F120 > Z120 > A120 > AC for CO_2, and F120 > A120 > Z120 > AC for CO. Therefore, the thermal stability of the AC-MO materials follows the general sequence F120 < Z120 < A120. Regarding H_2O, the desorbed amounts are very similar for the three samples, whereas the amounts of CO_2 and CO are by far very different. The dehydroxylation effect as compared to the dehydration effect is stronger for F120 and weaker for A120 and Z120, which must be highlighted as it is consistent with the higher

tendency of the Fe^{3+} ion than for the Al^{3+} and Zn^{2+} ions to undergo hydrolysis. It is also worth mentioning that the number of thermal effects easily visible to the naked eye in the MS profiles is higher by F120 > Z120 > A120 for CO_2 and by A120 > Z120 > F120 for CO. The variation of the hydrogen content (Table 2) also by A120 > Z120 > F120 strongly supports that CO in part, at least, desorbed from hydrogen containing groups, such as phenolic hydroxyl groups. However, the formation of intermediate structures containing chemical bonds such as C=O, C-O and M-O during the oxidation of the carbon by the metal oxide at high temperature should not be ruled out. Perhaps, the chemical changes produced during the thermal analysis were determined by the content and reactivity of such a metal oxide, after its formation when the samples were heat-treated from 25 to 900 ºC.

3.3.2.5. Sample S120

With regard to S120, the TG-DTG curves in Fig. 7(a) show four strong effects of mass loss at around 100, 350, 555, and 755 ºC. The high mass loss of 23.2 wt% between 25 and 900 ºC is in line with the MC of + 49 wt% for S120. The MS profiles in Fig. 7(b) display stronger peaks at 130 ºC for H_2O, 760 ºC for CO_2, and 780 ºC for CO. Also notice the shoulder at 255 ºC for H_2O and the weak peaks at 255, 340 and 555 ºC for CO_2 and at 525 ºC for CO. The mass of evolved gases is higher by CO_2 > CO > H_2O.

The shape of the H_2O profile for S120 is very similar to that for Z120 in Fig. 6(a), displaying a strong peak with a pronounced shoulder ascribable to dehydration and dehydroxylation processes. The carboxylic acid groups desorbing CO_2 below 600 ºC may be formed because of the action of powerful oxidizing agents generated in the process of $SnCl_2$ oxidation by dissolved O_2 in the presence of AC. According to the

literature [42], they are metastable or dative peroxides which are chemically characterized by high energy content and great instability. Also, AC may be oxidized by air during the oven-drying step in a reaction catalysed by SnO_2 as this metal oxide behaves as an oxidation catalyst [43]. On the other hand, the great CO_2 release at around 750 ºC is compatible with the direct carbothermal reduction of solid SnO_2 by

$$SnO_2 + C \rightarrow Sn + CO_2 \quad (5)$$

that takes place above 630 ºC [44]. Furthermore, as this reaction progressed with increasing heat treatment temperature during the thermal analysis of S120 and the presence of SnO_2 decreased, the reaction

$$SnO_2 + 2C \rightarrow Sn + 2CO \quad (6)$$

may also occur, which would account for the great desorption of CO at around 800 ºC for S120. Nevertheless, CO may also be generated by the reaction (7)

$$CO_2 + C \rightarrow 2CO \quad (7)$$

at high temperature. Although the CO profile does not show peaks in the temperature range 500 and 650 ºC the slight increase produced in desorption of CO between 500 and 550 ºC is indicative of the presence of C-O-Sn bonds in the sample.

From Figs. 7(a) it follows that the rate of mass loss was maximum at around 350 ºC whereas, as shown in Fig. 7(b), no maximum of evolved H_2O, CO_2 or CO is noted in the MS profiles of these gases in the neighbourhood of temperatures. Therefore, the aforesaid thermal effect should be due to the release of gases other than H_2O, CO_2 and CO. Likely, Sn was also formed at low temperature [45-47] and vaporized when heating above 231.93 ºC at which Sn melts [10]).

3.3.2.6. Sample T120

A characteristic of anatase is its thermal and chemical stability [48]. Under calcination typically at 600-700 ºC, metastable anatase transforms into thermodynamically stable rutile [49,50], which is also non-reactive and that can only be reduced with difficulty to non-stoichiometric oxide phases [51]. Furthermore, the carbothermal reduction of TiO_2 in hydrogen, argon and helium with formation of titanium oxycarbide starts at 1200 ºC [52]. The TG-DTG curves and MS profiles for T120 are plotted in Fig. 8. As expected, the mass loss between 25 and 900 ºC was only slightly higher for T120 than for AC. In the case of T120, the mass of desorbed gas was significantly lower for H_2O and noticeably higher for CO_2 and especially for CO. The decrease in water desorption is not surprising by allowing for the very low H content for T120. The enhanced release of CO_2 is attributable to AC oxidation with formation of CO_2-desorbing surface groups. Although the carbon may be oxidized by O_2 in the presence of TiO_2 during the process of preparation of T120, the thermal transformation of oxygen surface groups of AC during the subsequent TG-MS analysis of T120 should not be ruled out. Carbon dioxide may also desorb from T120 after chemisorption as CO_2^- and CO_3^{2-}or HCO_3^- on TiO_2 [53,54]. Regarding the release of CO, data of the chemical analysis obtained for T120 (see Table 2) suggest that surface groups other than phenolic hydroxyl groups were involved in the generation of this gas from T120. Perhaps, they are carbon-oxygen and/or titanium-oxygen surface groups formed when T120 was heat-treated at high temperature. In brief, the results obtained in the MS analysis of T120 seem to indicate that in the process of preparation of T120 gases such as O_2 and CO_2 interacted chemically with oxygen surface groups of AC and with TiO_2, respectively, and that this noticeably influenced the thermal behaviour of the sample.

Perhaps, after the support of TiO_2 on AC, there was no significant restriction to gas entrance and diffusion in AC porosity because of the large size of TiO_2 particles which caused only small changes in the microporous structure of AC [7].

3.3.2.7. Sample W120

The TG-DGT curves and MS profiles for W120 are shown in Figs. 9 (a) and 9(b), respectively. In the TG-DTG curves it can be seen that the strongest effect of mass loss commenced at around 750 ºC and that rate was maximum at approximately 815 ºC. The mass loss between 25 and 900 ºC was 3.68 wt%. The MS profiles exhibit a single peak at around 140 ºC for H_2O, two weaker peaks at 285 and 380 ºC for CO_2, and another very strong single peak at 830 ºC for CO. The amount of evolved gases varies by $CO > H_2O > CO_2$. As compared to AC, it can be noted that the amounts of evolved H_2O, CO_2 and CO are significantly higher for W120. These results are not surprising as H_2O is necessary to stabilize the microcrystalline structure of WO_3. Furthermore, the degree of hydration and hydroxylation of WO_3 may be enhanced during the storage period at room temperature [55]. Moreover, WO_3 monohydrate transforms into anhydrous WO_3 at around ~220-240 ºC [56]. On the other hand, WO_3 supported on activated carbon behaves as an oxidation catalyst for organic compounds [57], which may give rise to an increased desorption of CO_2 if AC was oxidized by oxygen chemisorbed on its surface. At temperature ≥ 700 ºC a crystallite growth was reported before [56]. It was accompanied with a great CO release, attributable to the carbothermal reduction of WO_3 [58]:

$$WO_3 + 3C \rightarrow W + 3CO \ (T > 700\ ºC) \quad (8)$$

and was explained on the basis of a high dispersion of WO_3 on the surface of AC. The resulting metallic tungsten may further react with AC to give tungsten carbides by the so-called carburization reaction [59]. In any event, by taking into account the MC of + 6 wt% for W120, the small mass loss of 3.68 wt% for W120 indicates that WO_3 was carbothermally reduced only to a reduced extent.

3.3.2.8. Comparison of S120, T120 and W120

As expected according to the MG produced in the preparation of the samples, the mass loss in the TG analysis is higher by S120 >> W120 > T120. The number of thermal effects varies by S120 = T120 > W120 for H_2O, S120 > W120 > T120 for CO_2 and T120 > S120 = W120 for CO. For H_2O, not only the variety of desorption effects but also the relative amounts of evolved H_2O depend on the sample. Thus, no dehydroxylation effect is observed for W120. Furthermore, the effect of dehydration or dehydroxylation is the strongest one for S120 and T120, respectively, which is indicative of a dissimilar thermal behaviour for both samples. The amounts of evolved H_2O, CO_2 and CO follow the sequence S120 >> W120 > T120.

4. Conclusions

From the above results obtained in the TG-MS analysis of the wide series of AC-MO materials prepared by wet impregnation of AC with Al^{3+}, Fe^{3+}, Zn^{2+}, $SnCl_2$, TiO_2 and WO_4^{2-} in water in two successive soaking and oven-drying steps, the following main conclusions may be drawn. The mass loss produced in the TG analysis is 1.35 wt% for AC, 2.16 wt% for ACB, and between 2.47 and 23.20 wt% for the AC-MO materials. It varies by S120 > F120 > A120 > Z120 > W120 > T120. Except for AC

and ACB, the mass of evolved gases as a rule is much higher for CO_2 and CO than for H_2O. Desorption of H_2O has been connected with dehydration and dihydroxylation processes and that of CO_2 with decarboxylation and other processes. The thermal desorption of CO at high temperature has been generally associated with the carbothermal reduction of metal oxides. The reaction gives rise to the formation of a low melting point metal such as Sn, Al or Zn which melts and vaporizes below 900 ºC with mass loss. The number of thermal effects desorbing CO_2 and CO is greater for A120, F120 and Z120 than for S120, T120 and W120. It is so in particular in the case of CO_2 for F120 and of CO for A120. Only for F120 and T120, the amount of desorbed water is larger by dehydroxylation than by dehydration. The masses of evolved H_2O, CO_2 and CO are by far higher for S120. However, they are lower for T120 and W120. The mass of evolved CO (mg) is 0.010 for AC, 0.328 for T120 and 1.454 for F120.

Acknowledgements

Financial support by Gobierno de Extremadura and European FEDER Funds is gratefully acknowledged. A. Barroso-Bogeat thanks Spanish Ministerio de Educación, Cultura y Deporte for the concession of a FPU grant (AP2010-2574).

References

[1] F. Rodríguez-Reinoso, Active carbon: Structure, characterization, preparation and applications, in: H. Marsh, E. A. Heintz, F. Rodríguez-Reinoso (Eds.), Introduction to Carbon Technologies, Universidad de Alicante, Alicante, Spain, 1997, pp. 35-101.

[2] P. Cheremisinoff, A.C. Morresi, Carbon adsorption applications, in: P. Cheremisinoff, F. Ellerbusch (Eds.), Carbon Adsorption Handbook, Ann Arbor Science, Ann Arbor, 1980, pp. 1-53

[3] M.O. Corapcioglu, C.P. Huang, The adsorption of heavy metals onto hydrous activated carbon, Wat. Res. 21 (1987) 1031-1044.

[4] H.P. Boehm, Acidic and basic properties of hydroxylated metals oxide surfaces, Discuss. Faraday Soc. 52 (1971) 264-275.

[5] C. Noguera, Polar oxide surfaces, J. Phys.: Condens. Matter. 12 (2000) R367-R410.

[6] A. Barroso-Bogeat, M. Alexandre-Franco, C. Fernández-González, V. Gómez-Serrano, FT-IR analysis of pyrone and chromene structures in activated carbon, Energy Fuels 28 (2014) 4096-4103.

[7] A. Barroso-Bogeat, M. Alexandre-Franco, C. Fernández-González, V. Gómez-Serrano, Preparation of metal oxides-activated carbon hybrid catalysts. Textural characterization, Fuel Process. Technol. 126 (2014) 95-103.

[8] A. Barroso-Bogeat, M. Alexandre-Franco, C. Fernández-González, V. Gómez-Serrano, Preparation and microstructural characterization of activated carbon-metal oxide hybrid catalysts: New insights into reaction paths, J. Mater. Sci. Technol. 31 (2015) 806-814.

[9] C.F. Baes, Jr., R.E. Mesmer, The Hydrolysis of Cations, John Wiley & Sons, New York, 1976.

[10] In: D.R. Lide (Ed.), CRC Handbook of Chemistry and Physics, 2005-2006 86th ed., Taylor & Francis, Boca Raton, 2005.

[11] A. Ortiz, M. Mendoza, J.E. Rodríguez Paez, Naturaleza y formación de complejos intermedios del sistema $SnCl_2$-NH_4OH-H_2O, Mater. Res. 4 (2001) 265-272.

[12] F. Séby, M. Potin-Gautier, E. Giffaut, O.F.X. Donard, A critical review of thermodynamic data for inorganic tin species, Geochim. Cosmochim. Acta 65 (2001) 3041-3053.

[13] H. Remi, Treatise on Inorganic Chemistry, Vol. 1, Elsevier, Amsterdam, 1956.[13]

[14] O.V. Reva, T.N. Vorob´eva, Oxidation, hydrolysis and colloid formation in storage of $SnCl_2$ aqueous solutions, Russ. J. Appl. Chem. 75 (2002) 700-705.

[15] W.F. Huang, H.T. Chen, M.C. Lin, The adsorption and reactions of $SiCl_\chi$(χ = 0-4) on hydroxylated TiO_2 anatase (101) surface: A computational study on the functionalization of titania with $Cl_2Si(O)O$ adsorbate, Comput. Theor. Chem. 993 (2012) 45-52.

[16] M. J. Freedman, Polymerization of anions: The hydrolysis of sodium tungstate and sodium chromate, J. Am. Chem. Soc. 80 (1958) 2072-2077.

[17] G.S. Szymanski, Z. Karpinski, S. Biniak, A. Swiatkowski, The effect of gradual thermal decomposition of surface oxygen species on the chemical and catalytic properties of oxidized activated carbon, Carbon 40 (2002) 2627-2639.

[18] H. Jankowska, A. Świątkowski, J. Choma, Active Carbon, Ellis Horwood, Chichester, 1991.

[19] C. Moreno-Castilla, M.A. Ferro-García, J.P. Joly, I. Bautista-Toledo, F. Carrasco-Marin, J. Rivera-Utrilla, Activated carbon surface modifications by nitric acid, hydrogen peroxide, and ammonium peroxydisulfate treatments, Langmuir 11 (1995) 4386-4392.

[20] I. Levin, D. Brandon, Metastable alumina polymorphs: Crystal structures and transition sequences, J. Am. Ceram. Soc. 81 (1998) 1995-2012.

[21] B.C. Lippens, J.J. Steggerda, Active alumina, in: B.G. Linsen (Ed.), Physical and Chemical Aspects of Adsorbents and Catalysts, Academic Press, New York, 1970, pp. 171-212.

[22] C. Morterra, G. Magnacca, A case study: Surface chemistry and surface structure of catalytic aluminas, as studied by vibrational spectroscopy of adsorbed species, Catal. Today 27 (1996) 497-532.

[23] V. Gómez-Serrano, F. Píriz-Almeida, C.J. Durán-Valle, J. Pastor-Villegas, Formation of oxygen structures by air activation. A study by FT-IR spectroscopy, Carbon 37 (1999) 1517-1528.

[24] K. Winter, D. Barton, The thermal decomposition of benzoic acid, Can. J. Chem. 48 (1970) 3797-3801.

[25] A.C. Gonzalez, C.W. Larson, D.F. McMillen, D.M. Golden, Mechanism of decomposition of nitroaromatics. Laser-powered homogeneous pyrolysis of substituted nitrobenzenes, J. Phys. Chem. 89 (1985) 4809-4814.

[26] H. Pines, W. O. Haag, Alumina: Catalyst and support: I. Alumina, its intrinsic acidity and catalytic activity, J. Am. Chem. Soc. 82 (1960) 2471-2483.

[27] A.M. Scheer, C. Mukarakate, D.J. Robichaud, M.R. Nimlos, H.-H. Carstensen, G.B. Ellison, Unimolecular thermal decomposition of phenol and d_5-phenol: Direct observations of cyclopentadiene formation via cyclohexdienone, J. Chem. Phys. 136 (2012) 044309. doi: 10.1063/1.3675902.

[28] V. Jayaram, Synthesis and characterization of metastable ceramic oxides, in: S. Banerjee, R.V. Ramanujan (Eds.), Advances in Physical Metallurgy, Gordon and Breach Inc., Pensylvania, 1996, pp. 455-460.

[29] A. van Zyl, M.M. Thackeray, G.K. Duncan, A.I. Kingon, The synthesis of beta alumina from aluminum hydroxide and oxyhydroxide precursors, Mat. Res. Bull. 28 (1993) 145-157.

[30] T. C. Chou, T. G. Nieh, Nucleation and concurrent anomalous grain growth of α-Al_2O_3 during γ→α phase transformation, J. Am. Ceram. Soc. 74 (1991) 2270-2279.

[31] G. Paglia, C. E. Buckley, A. L. Rohl, R. D. Hart, K. Winter, A. J. Studer, B. A. Hunter, J. V. Hanna, Bohemite derived γ-alumina system. 1. Structural evolution with temperature, with the identification and structural determination of a new transition phase, γ´-alumina, Chem. Mater. 16 (2004) 220-236.

[32] M. Halmann, A. Frei, A. Steinfeld, Carbothermal reduction of alumina: Thermochemical equilibrium calculations and experimental investigation, Energy 32 (2007) 2420-2427.

[33] V. Balek, J. Subrt, Thermal behaviour of iron(III) oxide hydroxides, Pure & Appl. Chem. 67 (1995) 1839-1842.

[34] N. Koga, S. Okada, T. Nakamura, H. Tanaka, A kinetic study of the thermal decomposition of iron(III) hydroxide-oxides. 2. Preparation and thermal decomposition of γ-FeO(OH), Thermochim. Acta 267 (1995) 195-208.

[35] F.W. Chukhrov, B.B. Zvyagin, L.P. Ermilova, A.I. Gorshov, New data on iron oxides in the weathering zone, in: J.M. Serratosa (Ed.), Proc. Int. Clay Conf., Div. de Ciencias, C.S.I.C., Madrid, 1970, pp. 333-341.

[36] T. Ishikawa, K. Inouye, The structural transformation of ferric oxyhydroxides and their activity to sulfur dioxide, B. Chem. Soc. Jpn. 45 (1972) 2350-2354.

[37] W. Lodding, L. Hammell, Differential thermal analysis of hydroxides in reducing atmosphere, Anal. Chem. 32 (1960) 657-662.

[38] P. Li, Z.P. Xu, M.A. Hampton, D.T. Vu, L. Huang, V. Rudolph, A.V. Nguyen, Control preparation of zinc hydroxide nitrate nanocrystals and examination of the chemical and structural stability, J. Phys. Chem. C 116 (2012) 10325-10332.

[39] W. Stählin, H.R. Oswald, The infrared spectrum and thermal analysis of zinc hydroxide nitrate, J. Solid State Chem. 2 (1971) 252-255.

[40] B.S. Kim, J.M. Yoo, J.T. Park, J.C. Lee, A kinetic study of the carbothermic reduction of zinc oxide with various additives, Mater. Trans., JIM 47 (2006) 2421-2426.

[41] M. Seredych, O. Mabayoje, M.M. Kolesnik, V. Krstic, T.J. Bandosz, Zinc (hydr)oxide/graphite based-phase composites: Effect of the carbonaceous phase on surface properties and enhancement in electrical conductivity, J. Mater. Chem. 22 (2012) 7970-7978.

[42] R.C. Haring, J.H. Walton, The autoxidation of stannous chloride. II A survey of certain factors affecting this reaction, J. Phys. Chem. 37 (1933) 133-145.

[43] M. Batzill; U. Diebold, The surface and materials science of tin dioxide. Review, Prog. Surf. Sci. 79 (2005) 47-154.

[44] A.M. Ikaev, O.S. Polezhaeva, P.G. Mingalev, G. V. Lisichkin, Reaction of diethyl bitane-1-phosphonate with the surface of tin dioxide, Russ. J. Gen. Chem. 78 (2008), 417-420.

[45] R. Padilla, The reduction of cassiterite with carbon, Ph.D. Thesis, University of Utah, 1977.

[46] J.C. Platteeuw, G. Meyer, The system tin + oxygen, Trans. Faraday Soc. 52 (1956) 1066-1073.

[47] E. Wilberg, A.F. Hollemann, Inorganic Chemistry, Elsevier, Amsterdam.

[48] M. Zhang, J. Wu, D.D. Lu, J. Yang, Enhanced visible light photocatalytic activity of TiO_2 nanotube array films by co-doping with tungsten and nitrogen, Int. J. Photoenergy 2013; http://dx.doi.org/10.1155/2013/471674.

[49] M. Sorescu, T. Xu, The effect of ball-milling on the thermal behavior of anatase-doped hematite ceramic system, J. Therm. Anal. Calorim. 103 (2011) 479-484.

[50] Y. Hu, H.-L.Tsai, C.-L. Huang, Effect of brookite phase on the anatase-rutile transition in titania nanoparticles, J. Eur. Ceram. Soc. 23 (2003) 691-696

[51] N.T. Nolan, M.K. Seery, S.C. Pillai, Spectroscopic investigation of the anatase-to-rutile transformation of sol-gel-synthesized TiO_2 photocatalysts, J. Phys. Chem. C 113 (2009) 16151-16157.

[52] M. A. R. Dewan, G. Zhang, O. Ostrovski, Carbothermal reduction of titania in different gas atmospheres, Metall. Mater. Trans. B 40 (2009) 62-69.

[53] D. J. C. Yates, Infrared studies of the surface hydroxyl groups on titanium dioxide, and of the chemisorption of carbon monoxide and carbon dioxide, J. Phys. Chem. 65 (1961) 746-753.

[54] M. Primet, P. Pichat, M.-V. Pathieu, Infrared study of the surface of titanium dioxides. II: Acidic and basic properties, J. Phys. Chem. 75 (1971) 1221-1226.

[55] C. G. Granqvist, Handbook of Inorganic Electrochromic Materials, Elsevier, Amsterdam, 2002.

[56] S. Supothina, P. Seeharaj, S. Yoriya, M. Sriyudthsak, Synthesis of tungsten oxide nanoparticles by acid precipitation method, Ceram. Int. 33 (2007) 931-936.

[57] M.A. Álvarez-Merino, M.F. Ribeiro, J.M. Silva, F. Carrasco-Marín, F.; Maldonado-Hódar, F.J., Activated carbon and tungsten oxide supported on activated carbon catalysts for toluene catalytic combustion, Environ. Sci. Technol. 38 (2004) 4664-4670.

[58] G.A. Swift, R. Koc, Tungsten powder from carbon coated WO_3 precursors, J. Mat. Sci. 36 (2001) 803-806.

[59] M.A. Álvarez-Merino, F. Carrasco-Marín, J.L.G. Fierro, C. Moreno-Castilla, Tungsten catalysts supported on activated carbon: I. Preparation and characterization after their heat treatment in inert atmosphere. J. Catal. 192 (2000) 363-373.

Figure Captions

Fig. 1. FT-IR spectra of AC and ACB.

Fig. 2. Thermal behaviour of AC: (a), TG-DTG curves; (b), MS profiles

Fig. 3. Thermal behaviour of ACB: (a), TG-DTG curves; (b), MS profiles.

Fig. 4. Thermal behaviour of AC and A120: (a), TG-DTG curves; (b), MS profiles.

Fig. 5. Thermal behaviour of AC and F120: (a), TG-DTG curves; (b) and (c), MS profiles.

Fig. 6. Thermal behaviour of AC and Z120: (a), TG-DTG curves; (b), MS profiles.

Fig. 7. Thermal behaviour of AC and S120: (a), TG-DTG curves; (b), MS profiles.

Fig. 8. Thermal behaviour of AC and T120: (a), TG-DTG curves; (b), MS profiles.

Fig. 9. Thermal behaviour of AC and W120: (a), TG-DTG curves; (b), MS profiles.

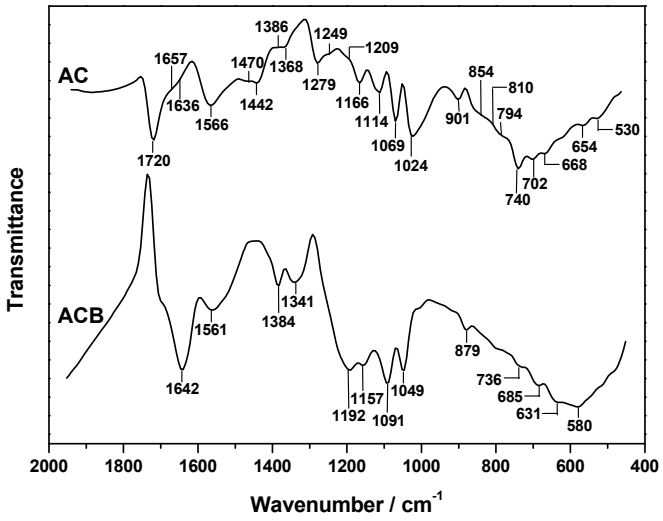

Fig. 1. FT-IR spectra of AC and ACB.

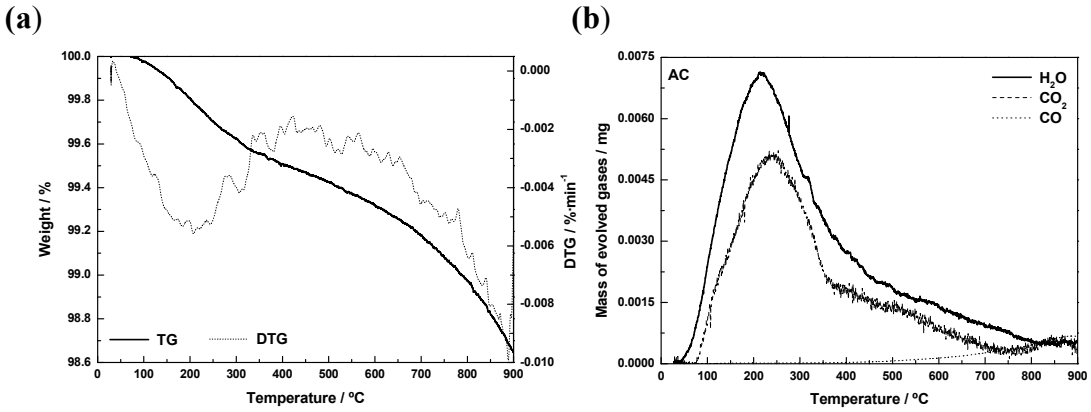

Fig. 2. Thermal behavior of AC: (a), TG-DTG curves; (b), MS profiles.

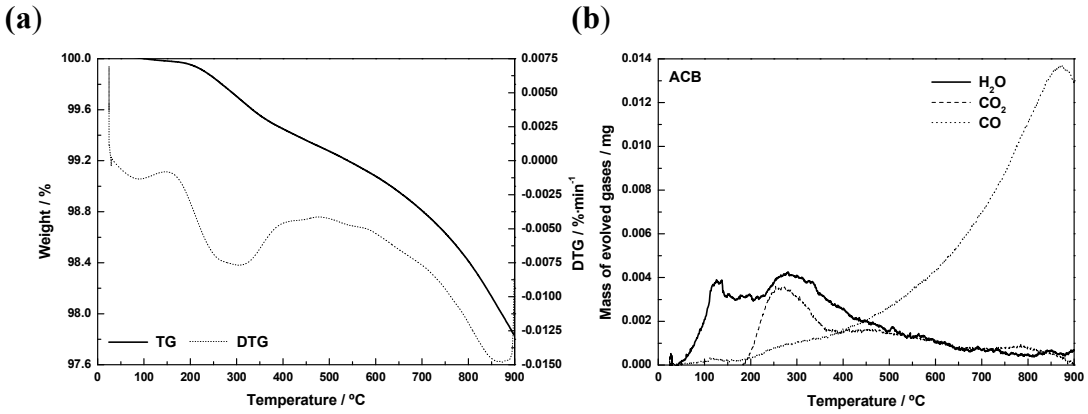

Fig. 3. Thermal behavior of ACB: (a), TG-DTG curves; (b), MS profiles.

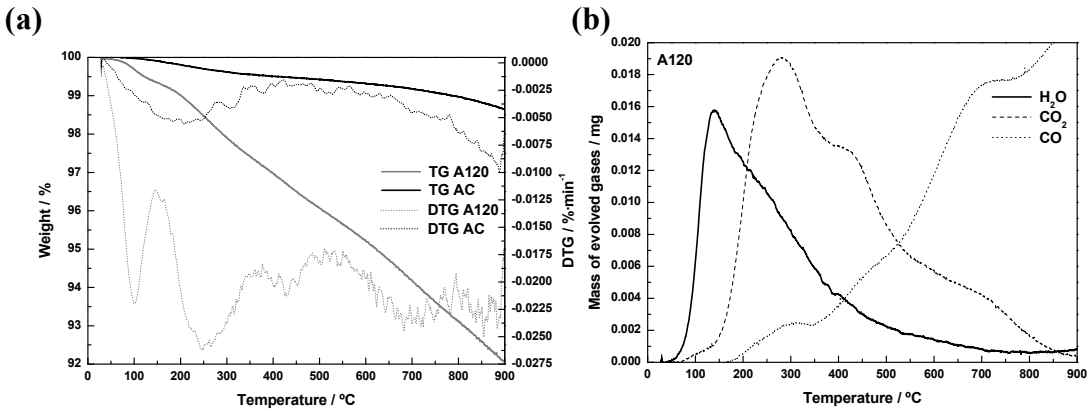

Fig. 4. Thermal behavior of AC and A120: (a), TG-DTG curves; (b), MS profiles.

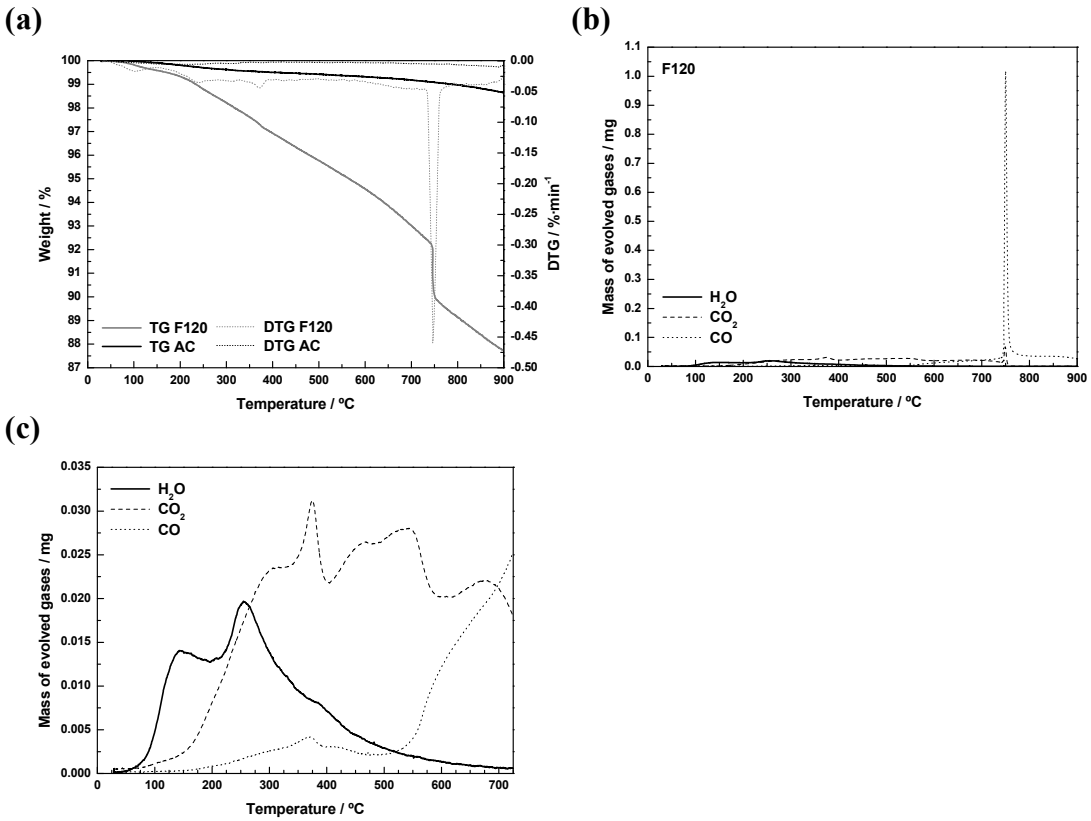

Fig. 5. Thermal behavior of AC and F120: (a), TG-DTG curves; (b) and (c), MS profiles.

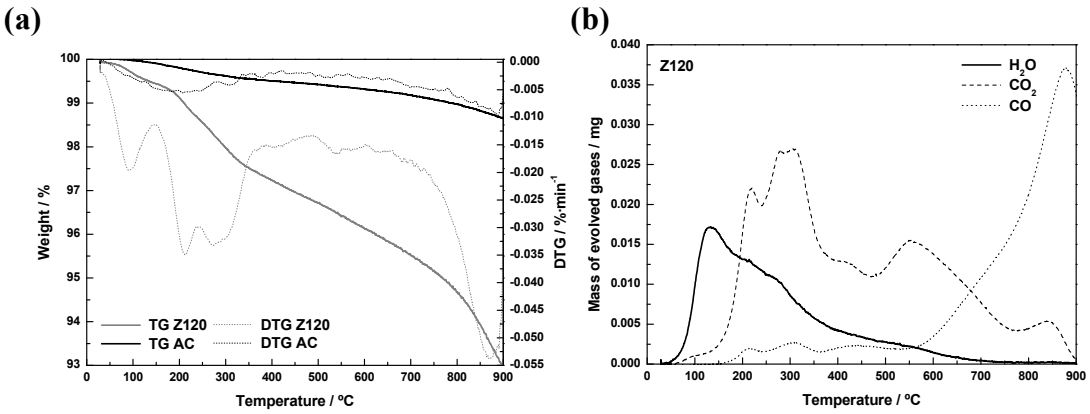

Fig. 6. Thermal behavior of AC and Z120: (a), TG-DTG curves; (b), MS profiles.

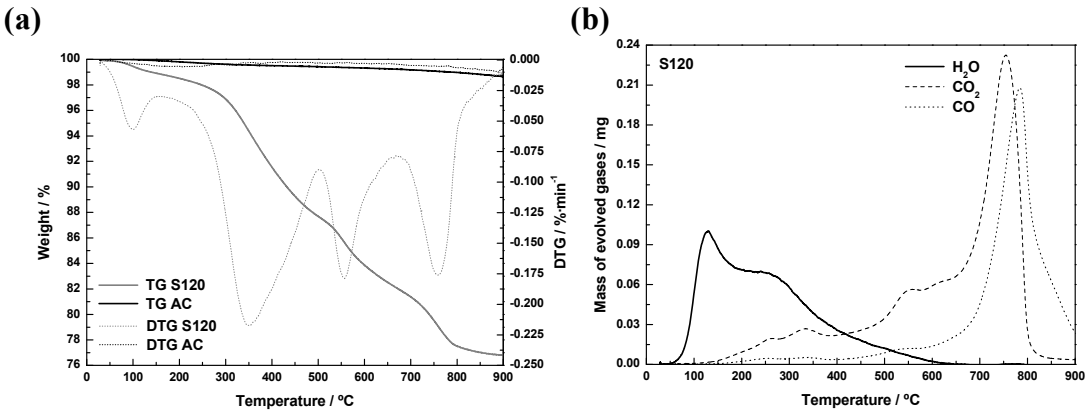

Fig. 7. Thermal behavior of AC and S120: (a), TG-DTG curves; (b), MS profiles.

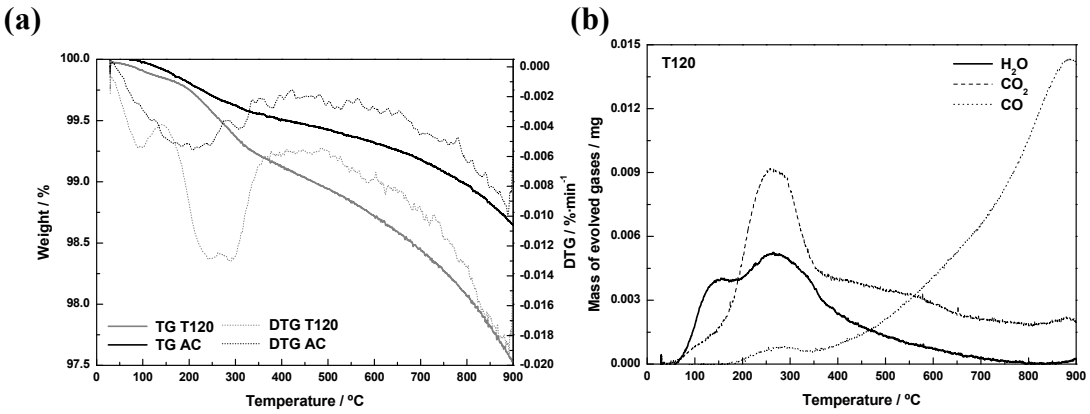

Fig. 8. Thermal behavior of AC and T120: (a), TG-DTG curves; (b), MS profiles.

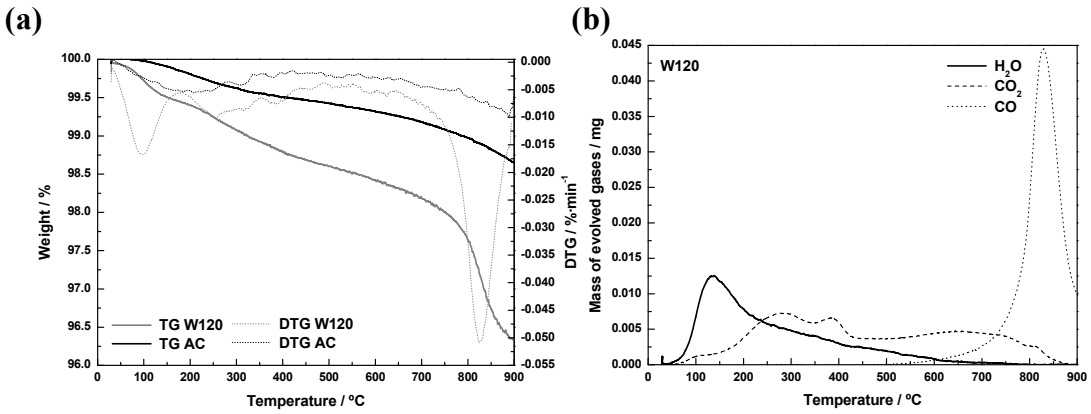

Fig. 9. Thermal behavior of AC and W120: (a), TG-DTG curves; (b), MS profiles.

Tables

Table 1. Preparation of AC-MO materials. Mass changes and sample codes.

Precursor	pH	MC / wt%	Code
$Al(NO_3)_3 \cdot 9H_2O$	2.91	2	A120
$Fe(NO_3)_3 \cdot 9H_2O$	1.54	14	F120
$Zn(NO_3)_2 \cdot 6H_2O$	5.16	3	Z120
$SnCl_2 \cdot 2H_2O$	1.37	49	S120
TiO_2 anatase	5.84	3	T120
$Na_2WO_4 \cdot 2H_2O$	9.54	6	W120

Table 2. Elemental analysis of the samples.

Sample	C / wt%	H / wt%	N / wt%	S / wt%	$O_{diff.}$ / wt%
AC	86.50	0.51	0.26	0.64	12.09
ACB	81.59	1.69	0.64	0.48	15.60
A120	72.83	1.16	0.49	0.56	24.96
F120	72.48	0.85	0.44	0.59	25.64
Z120	77.98	0.86	0.61	0.60	19.95
S120	52.32	1.25	0.06	0.37	46.00
T120	85.81	0.20	0.55	0.63	12.81
W120	78.32	0.98	0.20	0.61	19.89

Table 3. TG analysis of the samples. Mass loss between 25 and 900 ºC.

Sample	Mass loss / wt%
AC	1.35
ACB	2.16
A120	7.95
F120	12.27
Z120	7.02
S120	23.20
T120	2.47
W120	3.68

Table 4. MS analysis of the samples. Mass of evolved gases.

Sample	Mass of evolved gases / mg		
	H_2O	CO_2	CO
AC	0.210	0.110	0.010
ACB	0.150	0.100	0.350
A120	0.362	0.609	0.711
F120	0.457	1.285	1.454
Z120	0.388	0.903	0.624
S120	2.092	3.646	2.487
T120	0.152	0.283	0.328
W120	0.244	0.314	0.389